2009: The Journal of Astronomical Data 15, 1.

Photometric study of selected cataclysmic variables II. Time-series photometry of nine systems.

C. Papadaki[1,2], H.M.J. Boffin[3], V. Stanishev[4], P. Boumis[5], S. Akras[5,6] and C. Sterken[1]

(1) Vrije Universiteit Brussel, Pleinlaan 2, 1050 Brussels, Belgium
(2) ESO, Casilla 19001, Santiago 19, Chile
(3) ESO, Karl-Schwarzschild-Str. 2, 85748 Garching, Germany
(4) Department of Physics, Stockholm University, 106 91 Stockholm, Sweden
(5) Institute of Astronomy and Astrophysics, National Observatory of Athens, 15236 Athens, Greece
(6) University of Crete, Physics Department, 71003 Heraklion, Crete, Greece

Received June 4, 2008, accepted May 5, 2009

Abstract

We present time-series photometry of nine cataclysmic variables: EI UMa, V844 Her, V751 Cyg, V516 Cyg, GZ Cnc, TY Psc, V1315 Aql, ASAS J002511+1217.2, V1315 Aql and LN UMa. The observations were conducted at various observatories, covering 170 hours and comprising 7,850 data points in total.

For the majority of targets we confirm previously reported periodicities and for some of them we give, for the first time through photometry, their underlying spectroscopic orbital period. For those dwarf-nova systems which we observed during both quiescence and outburst, the increase in brightness was accompanied by a decrease in the level of flickering. For the eclipsing system V1315 Aql we have covered 9 eclipses, and obtained a refined orbital ephemeris. We find that, during this long baseline of observations, no change in the orbital period of this system has occurred. V1315 Aql also shows eclipses of variable depth.

1 Introduction

Cataclysmic variables (CVs) consist of a low-mass star filling its Roche lobe and transferring mass to its white-dwarf (WD) companion, a procedure resulting in the formation of an accretion disc. Due to their unpredictability and diversity leading to various types of CVs, these stars have since long been the subject of many studies.

Our aim is to better understand the properties of these systems by detecting periodicities and by analysing the various physical processes that occur, such as outbursts, superhumps, eclipses, flickering, etc. Our data will be useful for studying these CVs in the future, when a system possibly is in a different brightness state. In this study we present time-resolved photometric data of nine poorly-studied CVs, dwarf novae (DN) and nova-likes (NLs) in particular. A deeper study of five more CVs was published by Papadaki et al. (2006).

2 Observations

During the period 2002–2005 we conducted observations of several targets at five different observatories: the South African Astronomical Observatory (SAAO), the Observatorium Hoher List in Germany (OHL), Uccle Observatory (UC) in Belgium and two observatories in Greece: Kryoneri (KR) and Skinakas (SK). At the SAAO we used the 1-m telescope equipped with a back-illuminated 1024×1024, 24-μm pixel STE4 CCD camera with a field of view (FOV) of $5\farcm3 \times 5\farcm3$. At the OHL, we used the 1-m Cassegrain-Nasmyth telescope with the 2048×2048, 15-μm pixel HoLiCam CCD camera with a 2-sided read-out. We used the focal reducer and an effective FOV of $14\farcm1 \times 14\farcm1$. At UC we used the 0.85-m Schmidt telescope with a 2048×2048, 9-μm pixel Princeton Instruments TE CDD camera with a $30\farcm1 \times 30\farcm1$ FOV restricted to an effective FOV of $6\farcm1 \times 6\farcm1$ on average. At KR, the 1.2-m Cassegrain telescope with a 512×512 24-μm pixel CCD camera and a $2\farcm5 \times 2\farcm5$ FOV. Finally, we performed observations with the 1.3-m Ritchey-Chrétien telescope at SK, giving a FOV of $8\farcm5 \times 8\farcm5$ and used the 1024x1024 pixel SITe CCD camera.

While most of the observations were obtained without filter, the Johnson-R filter was occasionally used at SK. Table 1 gives the complete observing log for our 9 targets. The heliocentric Julian date (HJD) at the beginning of each observing night, as well as the total duration in hours, are also given. Fig. 1 gives the finding charts showing the selected comparison stars.

3 Data reduction

The CCD frames were processed for bias removal and flat-field correction. Small sets of bias frames were taken at regular time intervals during the night, and were then combined into one median nightly bias frame, which was then subtracted from all images. In case of significant changes in the CCD temperature, new bias frames were obtained at that point and neighbouring images were processed with the new

Table 1: Log of observations.

UT date	Site	HJD_{start}	Dur.	UT date	Site	HJD_{start}	Dur.
EI UMa				GZ Cnc			
09dec02⋆	OHL	2618.424	2.6	09mar03⋆	OHL	2708.394	2.8
10dec02	OHL	2619.417	7.7	16mar03⋆	UC	2715.451	0.7
31jan03⋆	OHL	2671.466	4.7	22mar03	UC	2721.369	0.7
31jan03⋆	UC	2671.459	5.0	25mar03	UC	2724.430	1.7
14feb03⋆	UC	2685.461	4.8				
16feb03	UC	2687.315	6.3	TY Psc			
17feb03	UC	2688.320	8.6	21jul03⋆	SK	2842.526	0.3
				22jul03	SK	2843.523	1.2
V844 Her				23jul03	SK	2844.491	1.9
04jul01⋆	UC	2095.423	3.2	10jan05⋆	OHL	3381.255	1.9
15may02⋆	UC	2410.497	2.0				
16may02	UC	2411.379	5.4	ASAS J0025+1217.2			
12jun02⋆	SK	2438.282	2.0	07oct04⋆	OHL	3286.333	1.7
14jun02	SK	2440.282	2.5	10oct04	OHL	3289.498	2.0
15jun02	SK	2441.282	2.5	11oct04	OHL	3290.423	1.8
V751 Cyg				V1315 Aql			
14may04⋆	OHL	3140.446	3.7	14aug03⋆	SAAO	2866.259	2.0
15may04	OHL	3141.448	0.7	15aug03	SAAO	2867.260	3.5
16may04	OHL	3142.444	3.5	16aug03	SAAO	2868.275	1.5
24may04⋆	OHL	3150.529	1.5	17aug03	SAAO	2869.224	4.2
26may04	OHL	3152.411	4.0	22aug04⋆	KR	3240.287	3.7
27may04	OHL	3153.411	4.0	31aug04⋆	SK	3249.242	5.4
28may04	OHL	3154.407	4.3	01sep04	SK	3250.254	5.2
29may04	OHL	3155.410	2.5	02sep04	SK	3251.267	4.5
07may05⋆	KR	3498.458	3.3				
08may05	KR	3499.455	3.5	LN UMa			
09may05	KR	3500.504	2.3	18feb03⋆	UC	2689.452	1.7
13may05	KR	3504.465	3.5	25feb03	UC	2696.288	9.2
				01jun04⋆	SK	3158.330	2.0
V516 Cyg				02jun04	SK	3159.375	1.4
08oct02⋆	UC	2556.319	3.5	06jun04	SK	3163.281	3.0
09oct02	UC	2557.331	2.8				
19oct02⋆	UC	2567.323	2.0				
23oct02	UC	2571.297	1.4				
05nov02	UC	2584.271	3.2				

Notes: $HJD_{start} = HJD - 2450000$; Dur. is the duration of each observing night in hours; all observations were obtained without filter, except for the SK measurements of V1315 Aql and LN UMa, which were made in Johnson-R; ⋆ at the UT date denotes the onset of each observing run.

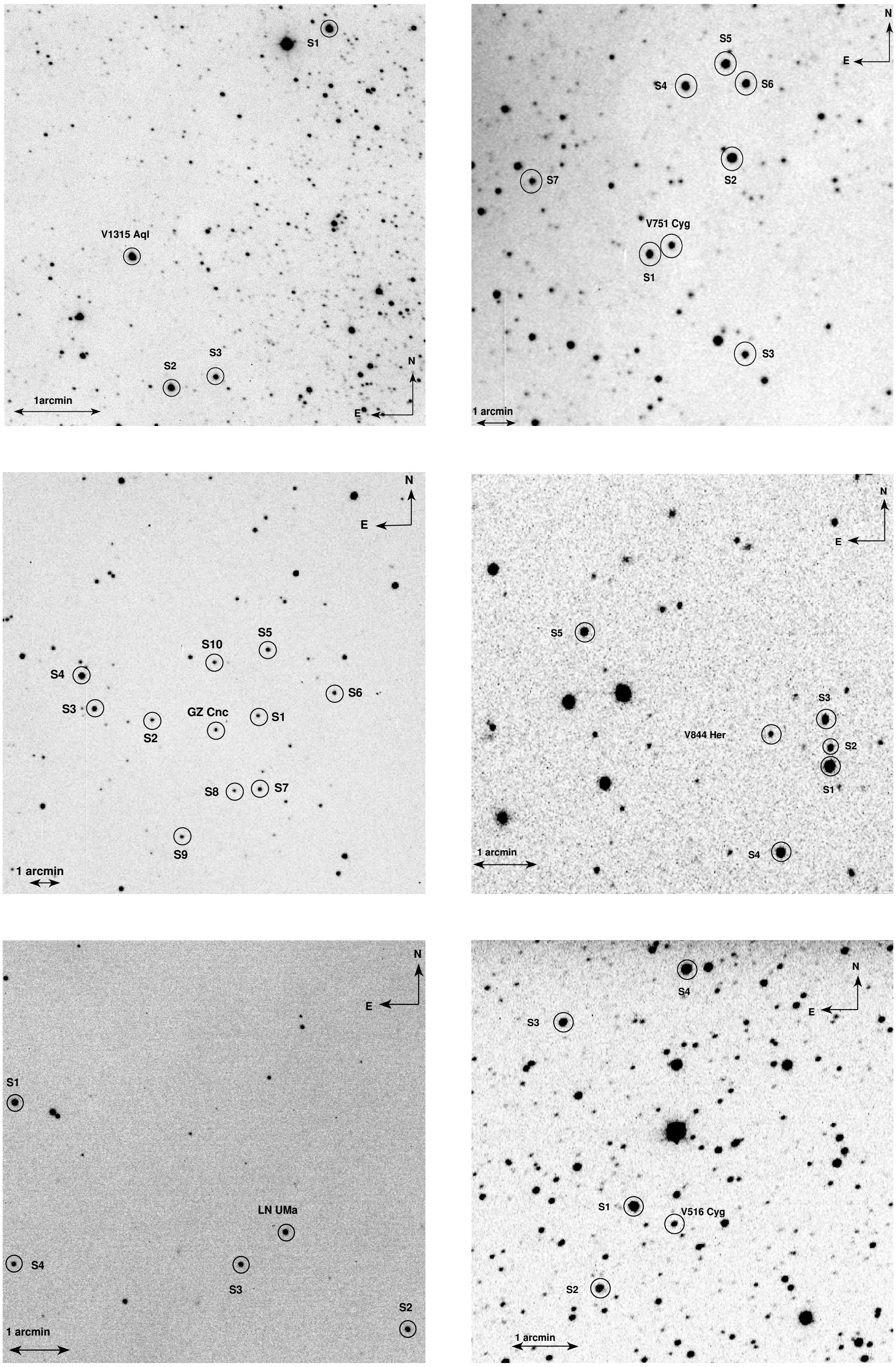

Figure 1: The finding charts of V1315 Aql, V751 Cyg, GZ Cnc, V844 Her, LN UMa and V516 Cyg. Marked on each chart are the comparison stars that served for differential photometry.

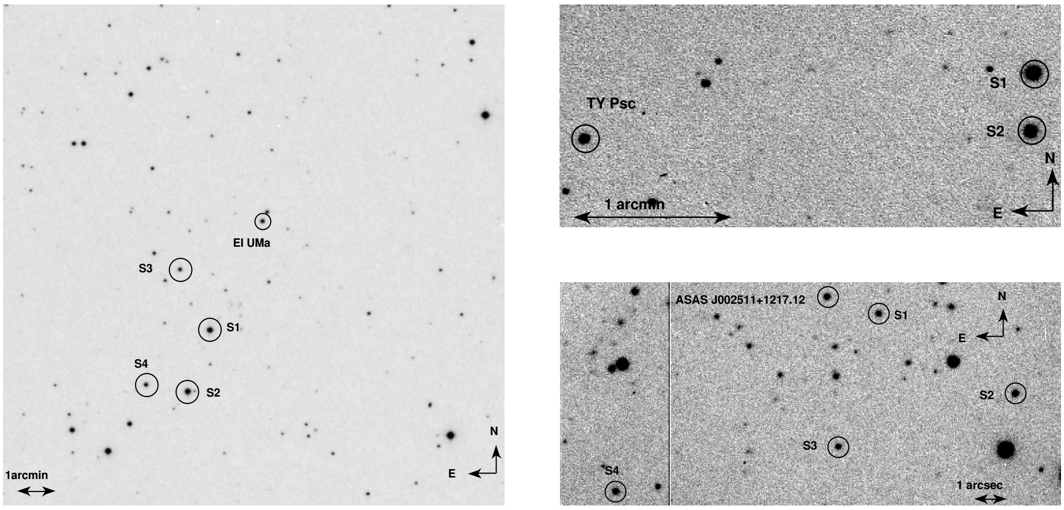

Figure 1: (continued) The finding charts of EI UMa, TY Psc and ASAS J002511+1217.2. Marked on each chart are the comparison stars that served for differential photometry.

combined bias frame. For each night we obtained a median flat-frame. In case of bad weather during both evening and morning twilight, the flat frame of the closest observing night was used.

Aperture photometry was performed using the IRAF package `apphot`. The circular aperture radius used for the computation of the instrumental magnitudes was equal to $2 \times FWHM$. When the nights were photometric and stable, a mean $FWHM$ was calculated, resulting in a fixed nightly aperture. In case of unstable sky quality with strongly variable seeing (as measured by $FWHM$), the night was divided into parts and each part was treated independently by calculating the corresponding aperture. After extracting the instrumental magnitudes of the CV and the selected comparison stars, the following procedure was applied in order to check the constancy of the comparison stars. The behaviour of the instrumental differential magnitudes of the comparison stars throughout the campaign was checked and compared to the difference of the instrumental magnitudes between the CV and one comparison star. This was done by plotting the differential magnitudes against time. Only when the series of differential magnitudes of a set of comparison stars did not reveal any night to night trend, and when the standard deviation σ of the comparison stars' differential magnitudes was at least 3 times smaller than that of the CV were the corresponding comparison stars retained for further use. Differential photometry was then applied according to the following procedure. We first calculated the average instrumental magnitude of each comparison star along with its σ and then determined the weighted average of the instrumental magnitudes of all comparison stars. The weights for each comparison star were set equal to the inverse of their σ, and the differential magnitudes of each CV were then obtained by subtracting the weighted average magnitude from the corresponding instrumental magnitude of the CV.

Given the fact that no filters were used, or if used had to be compared to data obtained without filters, it was not possible to obtain proper transformations to a photometric system. However, the following procedure, that yields the most reliable magnitudes in our case and provides the possibility of comparing to future or past data, was applied. From the comparison stars we chose those for which Henden & Honeycutt (1995) give V magnitudes. If their catalogue did not contain the required stars, the respective magnitudes were taken from the online USNO-A2.0 (United States Naval Observatory) catalogue at ESO (European Southern Observatory) science archive facility. For each observing night the catalogued magnitude of each comparison star was plotted against the differential magnitude (resulting from the mean of its differential magnitudes throughout the night) and a linear form was fitted by least squares. If all nights belonged to the same observing run (defined as the continuous period of allocated nights at a specific observing site) then a mean equation was calculated and therefore the differential magnitudes of our CV were transformed to magnitudes that are approximately on the magnitude scale of the catalogue. When observing runs at different sites were involved, the behaviour of the magnitude difference between two comparison stars (common in the FOV of all observing runs) was checked and the appropriate magnitude shift was applied. In this way we were able to compare all light curves obtained at different observatories.

The same reduction technique and light curve generation was applied to all CVs examined in this study. Table 2 gives the designations of the comparison stars used for each target, as seen in Fig. 1, along with their magnitudes and source from the literature. Whenever any offset occurs it will be stated in the corresponding section.

For comparison reasons and in order to have an impression of the range of each system's nightly mean-brightness variations, Table 3 gives $\mu_{\rm CV}$, which is each system's mean nightly magnitude, and $\mu_{\rm dif}$, the mean nightly differential magnitude between two comparison stars common in the FOV of all observing runs. The comparison stars, from which $\mu_{\rm dif}$ is calculated for each case, are also given.

In addition, when plotting the light curves of all objects in the next sections, an error bar is shown in the box of each night's light curve. This serves as an estimation of the error on a single measurement of the magnitude of the CV and is represented by the standard deviation around the mean of the differential magnitudes between two comparison stars, or else, the scatter in magnitude differences of two comparison stars. Concerning the choice of the comparison stars, we gave no preference over stars of smaller scatter for a given magnitude. As long as they fitted the criteria to be chosen (as mentioned earlier in this section), then they were equally treated for the rest of the procedure. The two stars should ideally be of similar magnitude as that of the CV. Otherwise, the use of comparison stars that are much fainter (brighter) would lead to overestimation (underestimation) of the error. However, there are cases where the magnitudes of the available comparison stars differ by 0.5–2 mag from that of the CV. In such cases, it was necessary to adopt the following procedure, in order to provide a realistic error estimate. Two pairs of comparisons stars, one pair with magnitudes similar to that of the CV, the other pair with magnitudes similar to the comparisons we have in the night of interest were looked for in another observing night, taking Table 2 into account. Let σ_1 and σ_2 be the scatter in magnitude differences for the two pairs, respectively, and σ be the scatter in magnitude differences of the comparisons in the night of interest. Then, the error on a single measurement is well represented by the quantity $\sigma^{'} = \frac{\sigma_1}{\sigma_2}\sigma$, and is demonstrated by the error bar in each light curve. Also, it should be pointed out that due to the change of the FOV between different observing runs of the same CV, the selected pairs of comparison stars are not necessarily the same between all observing runs of the same target.

As will be easily noticed from the error bars of the light curves in the upcoming sections, in most of the cases there are small variations between the nights. These variations are expected due to variations of the weather and therefore atmospheric conditions. Furthermore, if one CV appears in quiescence during one observing run and in outburst during another, the error is expected to decrease supposing there are not any great differences in the atmospheric conditions. However, the observing site of UC is always subjected to greater errors than the other sites because UC is located in a suburb of Brussels and therefore operates under much poorer atmospheric conditions compared to the rest of the observing sites we used. In addition, its low altitude makes it even more vulnerable to the variations of the lower atmosphere. These are the reasons of the large variance in the errors shown for some CVs. For V844 Her and LN UMa, the error estimation at UC is 10 and 4 times, respectively, greater than that at SK. For EI UMa, which we observed simultaneously and under good weather conditions at UC and HL, we found that the error at UC is 3.5 times greater than that at HL. V516 Cyg, observed only at UC, also shows an increase in the error but this is attributed not only to poorer atmospheric conditions but most predominantly to its decrease in brightness by 2 mag.

4 EI UMa

EI UMa (PG 0834+488) was discovered in the Palomar-Green survey (Green et al., 1982) and was classified as a CV on the basis of its optical spectrum which showed Balmer and high-excitation emission lines. Emission from high-excitation lines is characteristic of magnetic CVs. Cook (1985), in the first X-ray study of this target, found that EI UMa is a hard X-ray source with a low column-density and a ratio of X-ray to optical density resembling that of DN CVs. This, combined with the facts that the value of the column density matched that of non-magnetic CVs and, most importantly, that there was no X-ray modulation, drew him to the conclusion that EI UMa better matches a DN. One year later, Thorstensen (1986) performed the first radial-velocity study and detected a 6.4-h orbital period ($P_{\rm orb}$), the spectrum resembling that of a DN. On the other hand, he was of the opinion that the rather strong HeII λ4686 emission, the X-ray characteristics and the system magnitude,

Table 2: Designation of comparison stars.

EI UMa		GZ Cnc	
S1: [HH95] EI UMa-10	V=13.406	S1: U0975_06195484	R=15.7
S2: [HH95] EI UMa-4	V=13.403	S2: U0975_06196461	R=15.5
S3: [HH95] EI UMa-23	V=15.922	S3: U0975_06197019	R=14.0
S4: [HH95] EI UMa-32	V=15.168	S4: U0975_06197135	R=13.0
		S5: U0975_06195399	R=14.7
V844 Her		S6: U0975_06194753	R=15.1
S1: U1275_08930994	R=13.5	S7: U0975_06195450	R=14.9
S2: U1275_08930976	R=15.7	S8: U0975_06195694	R=15.9
S3: U1275_08931020	R=15.4	S9: U0975_06196184	R=15.4
S4: U1275_08931359	R=14.4	S10: U0975_06195886	R=15.3
S5: U1275_08932829	R=14.7		
		TY Psc	
V751 Cyg		S1: [HH95] TYPsc-24	V=15.240
S1: [HH95] V751Cyg-7	V=13.552	S2: [HH95] TYPsc-23	V=15.925
S2: [HH95] V751Cyg-3	V=12.284		
S3: U1275_14247362	R=14.3	ASAS J002511+1217.2	
S4: U1275_14251141	R=12.2	S1: U0975_00086988	R=15.9
S5: U1275_14248730	R=12.3	S2: U0975_00086066	R=15.4
S6: U1275_14247527	R=13.7	S3: U0975_00087221	R=16.0
S7: U1275_14260111	R=16.3	S4: U0975_00088736	R=16.1
V516 Cyg		V1315 Aql	
S1: U1275_14143883	R=13.9	S1: [HH95] V1315Aql-23	V=14.895
S2: U1275_14144823	R=14.7	S2: [HH95] V1315Aql-38	V=15.992
S3: U1275_14145851	R=14.8	S3: U0975_14381457	R=16.3
S4: U1275_14142515	R=13.6		
		LN UMa	
		S1: [HH95] PG1000+667-13	V=14.307
		S2: [HH95] PG1000+667-22	V=15.527
		S3: [HH95] PG1000+667-21	V=15.859
		S4: [HH95] PG1000+667-19	V=16.209

Notes: Designations starting with HH95 refer to stars as taken from Henden & Honeycutt (1995). The rest are adopted from the USNO-A2 catalogue.

implied a possible DQ Her type. One night of photoelectric photometry (Wilson et al., 1986) showed small amplitude flickering but no larger-amplitude long-term modulations.

Our dataset consists of observations obtained at OHL (3 nights) and at UC (3 nights). All observations were obtained without filter, and the exposure time varied from 45 to 90 sec. Because of the absence of a common couple of comparison stars

Table 3: Long-term behaviour.

UT date	$\mu_{CV} \pm \sigma_{CV}$	$\mu_{dif} \pm \sigma_{dif}$	UT date	$\mu_{CV} \pm \sigma_{CV}$	$\mu_{dif} \pm \sigma_{dif}$
EI UMa OHL		$\mu_{(S4-S1)}$	GZ Cnc		$\mu_{(S1-S2)}$
09dec02	15.096±0.054	1.694±0.012	09mar03	15.415±0.140	0.193±0.046
10dec02	14.964±0.079	1.688±0.013	16mar03	13.911±0.070	0.205±0.143
31jan03	14.564±0.044	1.721±0.018	22mar03	15.223±0.044	0.231±0.054
			25mar03	14.545±0.098	0.221±0.123
EI UMa UC		$\mu_{(S3-S1)}$			
31jan03	14.573±0.050	2.510±0.044	TY Psc		$\mu_{(S2-S1)}$
14feb03	15.057±0.039	2.238±0.031	21jul03	17.695±0.076	0.612±0.004
16feb03	14.431±0.037	2.232±0.034	22jul03	17.514±0.106	0.599±0.008
17feb03	14.451±0.046	2.239±0.023	23jul03	17.597±0.100	0.604±0.003
			10jan05	14.066±0.051	0.518±0.013
V844 Her		$\mu_{(S4-S1)}$			
04jul01	16.403±0.185	0.879±0.019	J002511		
15may02	16.454±0.102	0.881±0.012	+1217.2		$\mu_{(S1-S2)}$
16may02	16.420±0.105	0.882±0.011	07oct04	15.604±0.062	0.392±0.025
12jun02	16.136±0.046	0.897±0.003	10oct04	15.672±0.133	0.342±0.033
14jun02	16.097±0.082	0.872±0.009	11oct04	15.761±0.066	0.355±0.021
15jun02	16.204±0.044	0.869±0.007			
			V1315 Aql		$\mu_{(S2-S1)}$
V751 Cyg		$\mu_{(S7-S1)}$	14aug03	15.134±0.075	0.560±0.004
14may04	14.291±0.051	1.572±0.019	15aug03	14.552±0.082	0.568±0.008
15may04	14.401±0.060	1.541±0.024	16aug03	15.111±0.084	0.567±0.004
16may04	14.458±0.050	1.536±0.022	17aug03	14.987±0.093	0.562±0.004
24may04	14.324±0.053	1.534±0.038	31aug04	14.839±0.096	0.613±0.007
26may04	14.320±0.059	1.544±0.024	01sep04	14.882±0.124	0.612±0.007
27may04	14.403±0.052	1.551±0.023	02sep04	14.796±0.161	0.616±0.006
28may04	14.356±0.051	1.545±0.023			
29may04	14.304±0.066	1.547±0.038	LN UMa		$\mu_{(S3-S2)}$
07may05	14.606±0.069	1.641±0.018	18feb03	15.308±0.055	0.242±0.040
08may05	14.427±0.088	1.633±0.015	25feb03	15.207±0.056	0.253±0.033
09may05	14.318±0.058	1.634±0.009	01jun04	15.401±0.018	0.264±0.008
13may05	14.407±0.065	1.624±0.015	02jun04	15.343±0.021	0.261±0.012
			06jun04	15.293±0.026	0.265±0.006
V516 Cyg		$\mu_{(S2-S1)}$			
08oct02	13.585±0.013	1.008±0.024			
09oct02	13.609±0.013	1.012±0.022			
19oct02	15.304±0.064	1.004±0.019			
23oct02	15.806±0.040	1.007±0.013			
05nov02	15.885±0.078	0.987±0.022			

Notes: μ_{CV} and σ_{CV} are the mean nightly magnitude and corresponding σ of each CV ; μ_{dif} and σ_{dif} are the mean nightly differential magnitude and corresponding σ between two comparison stars. At the top of each μ_{dif} column, μ_{dif} is explicitly written, indicating which comparison stars were used in each case.

at the two sites, the overlapping observing night of 31 January 2003 was used for the comparison between the OHL and UC light curves. This was done by equating the mean magnitude of our system in the overlapping period of time in the common observing night. The light curves are shown in Fig. 2. The OHL and UC observing nights in Table 3 are separated since $\mu_{\rm dif}$ does not correspond to the same couple of comparison stars.

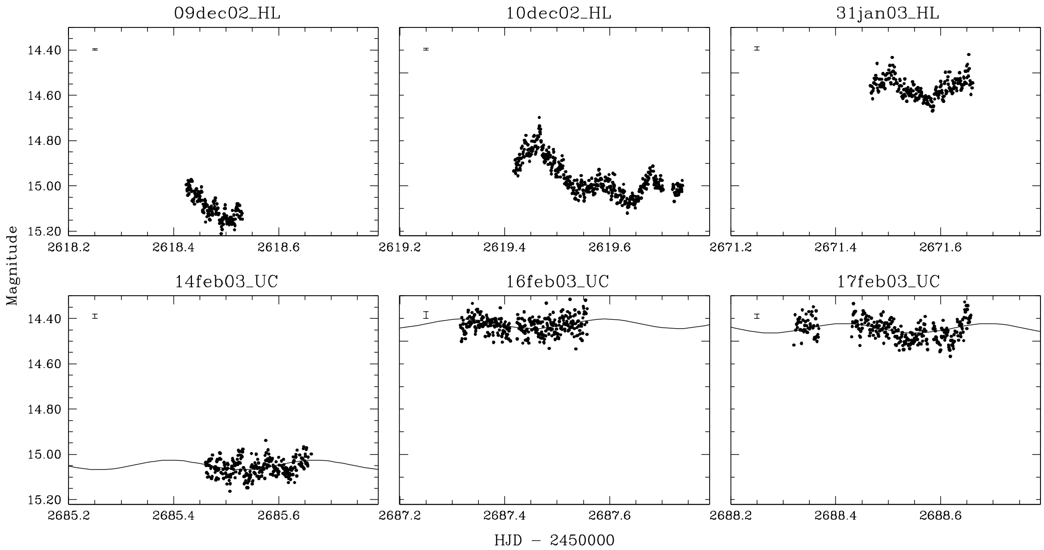

Figure 2: EI UMa light curves. In the upper left part of each light curve the error on a single measurement is indicated. The sine curve with $P = 3.598\,\mathrm{cd}^{-1}$ is superimposed on the UC light curves.

In Fig. 2 it is evident that the system's brightness, if we define two subsets, one for each observing site, showed an increase by ≈0.6 mag in both subsets. Table 3 illustrates the significancy of this increase since the variation of the mean differential magnitude between the comparison stars is of a much smaller scale. However, we also notice that between the two subsets, a great change in the system's variability occurs. For the subsequent analysis we have therefore treated the two subsets independently.

For EI UMa, as well as the remaining CVs that are presented in this study, frequency analysis was carried out by using the `period04` package (Lenz & Breger, 2005), based on the Discrete Fourier Transform method. The calculation of the uncertainties of the corresponding parameters was performed by means of Monte Carlo simulations from the same package. Before performing the frequency analysis, the trend in the light curves was removed by bringing them around their nightly mean. For the OHL subset we find a frequency of $2.7911\pm0.0002\,\mathrm{cd}^{-1}$ with a semi-amplitude of 0.076 ± 0.002 mag, along with the second highest peak, its $3.79\,\mathrm{cd}^{-1}$ alias, which corresponds to the frequency of the spectroscopic $P_{\rm orb}$. This suggests that even though our data are better fitted by a frequency of $2.7911\pm0.0002\,\mathrm{cd}^{-1}$, the $3.79\,\mathrm{cd}^{-1}$ alias (corresponding to the spectroscopic period) is more likely the right one. When running frequency analysis on the residuals, a frequency of $9.57\,\mathrm{cd}^{-1}$ or 2.5 h shows up. However, this signal does not occur on a stable time-scale and its folding is not promising. If we also consider that the duration of each OHL observing night is more or less a multiple of 2.5 h, then it is quite possible that $9.57\,\mathrm{cd}^{-1}$ is an alias frequency caused by the observing strategy.

The UC subset has more to reveal. We have detected a modulation at $3.640 \pm 0.011\mathrm{cd}^{-1}$ (Fig. 3a) or 6.59 h which agrees with the spectroscopic $P_{\rm orb}$ of 6.43 h and semi-amplitude of 0.021±0.002 mag. Moreover, it is true that had the periodicity not been detected spectroscopically, it would have been difficult to trust it. The sinusoidal representation of the periodicity has been superimposed on the UC light curves of Fig. 2. Fig. 3b shows the data folded on the 6.6-h periodicity, while Fig. 3c shows the folded data after applying 0.005 phase binning.

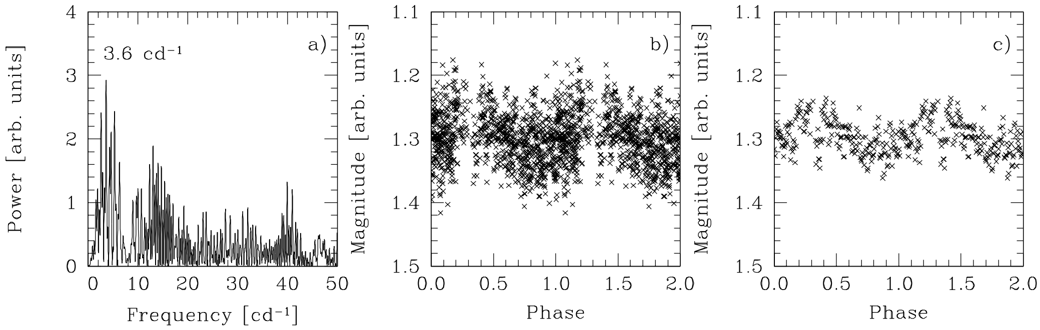

Figure 3: a) Resulting power spectra of the UC subset with the dominant frequency indicated b) Data folded on the 6.67-h periodicity c) Folded data, after 0.005 phase binning.

The standard deviation σ of the measurements in each light curve was also calculated. Then the average of all σ and its σ as uncertainty, were computed for both subsets. For the OHL subset it was found equal to 0.059±0.018 and for the UC subset 0.043±0.006. This implies a decrease in the level of flickering with the increasing brightness between the two subsets, a behaviour also noticed between the individual nights. Since the decrease in the level of flickering was followed by an increase on the errors of a single measurement, as indicated in the upper left corners of the light curves, this makes us more confident that it is indeed the level of flickering that has changed.

5 V844 Her

V844 Her is a DN discovered by Antipin (1996) on photographic plates. The best observed outburst lasted between 12 and 18 days. Since then, various variable star organisations followed this object. During its first outburst, clear superhumps were visible (Scovil, 1996; Vanmunster, 1996) and during a superoutburst a period of

0.056±0.001 d was found. More precise measurements of the superhump period (P_{sh}) are given by Kato & Uemura (2000) and Thorstensen et al. (2002) during the 1999 and 1997 outbursts, respectively. As Thorstensen et al. (2002) noted, the eruption timescale, a maximum brightness plateau of more than 10 d with a following rapid decrease in 1–2 d, as well as the superhumps establish the star's membership in the SU UMa class of DN. Quiescent spectra, part of the same study, appeared typical of those of DN and had double-peaked emission lines. The P_{orb}, measured from the Hα emission-line velocities, was found to be $0.054643\pm7\cdot10^{-6}$ d.

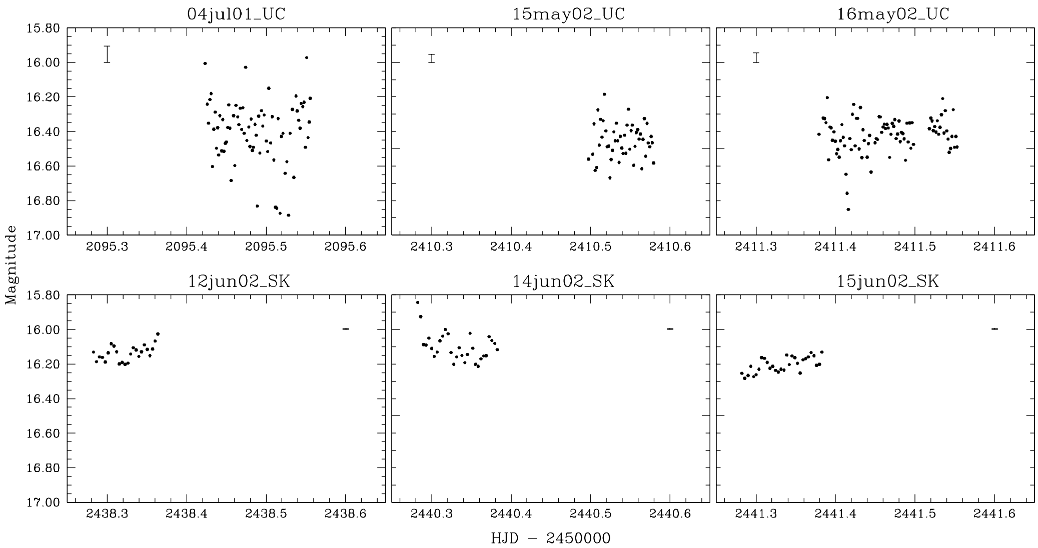

Figure 4: V844 Her light curves. In the upper left (or right) corner of each light curve the error on a single measurement is indicated.

V844 Her was observed during 3 nights at UC and during 3 nights at SK, all data obtained without filter. The exposure time varied between 120 and 240 sec. The light curves are shown in Fig. 4. The error bars on the upper left (or right) corners of each light curve indicate the error on a single measurement.

We performed frequency analysis, but no significant periodicity was detected. The σ of the measurements is 0.131±0.047 mag for the UC subset and 0.057± 0.022 mag for the SK one. However, the error on a single measurement, as indicated in the upper left part of each light curve in Fig. 4, is larger in the UC subset by a similar factor as the difference in σ between the two subsets. Thus we do not think that the flickering level between the two subsets has significantly changed.

An inspection of the AAVSO long-term light curves[1] revealed that we have just missed a superoutburst in the meantime between the second and third observing run. The nights of 15 and 16 May 2002 are placed just before the start or at the

[1]The AAVSO light curve generator tool is at www.aavso.org/data/lcg/. Using as input JD 245 2400–2450 and using only the visual-validated data, the superoutburst light curve is generated. Another superoutburst light curve with a more complete coverage is found for JD 245 2150–2181.

rising part of the superoutburst. During the nights of 12–15 June 2002 the system had returned to quiescence.

6 V751 Cyg

V751 Cyg (EM* LkHα) lies near the "eye" of the Pelican nebula (IC 5070). Its variability was discovered by Martynov (1958) and the star was initially believed to be an R Coronae Borealis star. Later spectra (Herbig, 1958; Herbig & Kameswara Rao, 1972) revealed its CV nature. This system had already shown drops up to 2.5 mag, but it was only after high-speed photometry was obtained, that it was first suggested to be a NL of the VY Scl subtype (Robinson et al., 1974). This suggestion was later confirmed by Downes et al. (1995) and Munari et al. (1997), on the basis of spectra showing Balmer and He emission (or emission cores in some cases), albeit not of great strength except Hα. V751 Cyg was also identified, during a low state, as a transient supersoft X-ray source (Greiner et al., 1999). X-ray observations during the high state showed that this was not the case. An anti-correlation of X-ray and optical intensity was also observed. Optical spectra during the same low-state revealed a very blue continuum and strong emission lines (Balmer, HeI and HeII λ4686).

The first detailed spectrophotometric study was published by Patterson et al. (2001). They reported photometric cycles at 3.348 h or $f_1 = 7.170 \pm 0.003\,\mathrm{cd}^{-1}$ and 3.9 d or $f_2 = 0.254 \pm 0.005\,\mathrm{cd}^{-1}$ as well as a modulation of the radial velocities at 3.468 h. These signals were identified as a negative superhump period P_{sh}^{-}, the wobbling period of a tilted accretion disc P_{wob} and P_{orb}, respectively. Occasionally the system showed P Cygni absorption profiles in the Balmer and HeI lines, correlated with the binary phase.

Our dataset consists of 8 nights of observing at OHL and 4 nights at KR. All observing nights were done without filter, and the exposure time varied between 20 and 80 sec, depending on the telescope and atmospheric conditions. The light curves are shown in Fig. 5.

The photometric frequencies, found by Patterson et al. (2001), are also detected in our data, albeit as their aliases or harmonics in some cases. Before applying frequency analysis, our dataset was divided into 3 subsets, one for each observing run. In all cases we cannot directly detect the low frequency f_2. In the first subset we find its 3$^{\mathrm{rd}}$ harmonic, in the second its 1.27 cd^{-1} alias and in the third its 2.21cd^{-1} alias. In contrast to Patterson et al. (2001), the number of each subset's consecutive observing nights is not larger than 4. This makes the direct detection of the ≈4-d P_{wob} more difficult. Performing period analysis on the residuals revealed the existence of P_{sh}^{-}. The corresponding frequencies for the first, second and third subset are 7.739±0.005, 6.171±0.002 and 9.144±0.004 cd^{-1}, respectively. The first signal reflects the combination of frequencies $f_1 + 2f_2$ (or an harmonic of the first frequency found in the same subset), and the other two aliases of f_1. The power spectra of the original and residual data are shown in the top and bottom row of

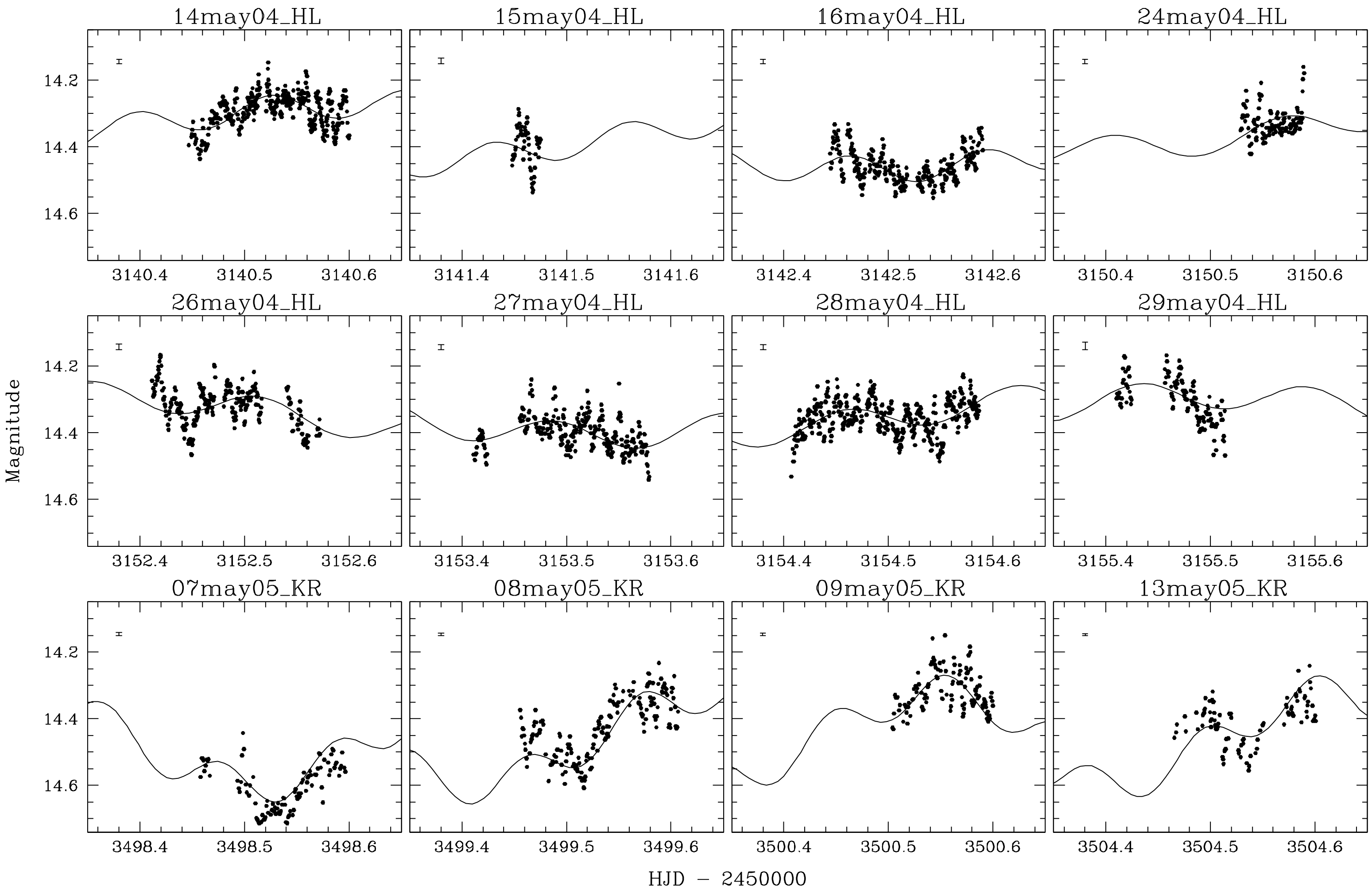

Figure 5: V751 Cyg light curves with the corresponding errors indicated in the upper left corner of each light curve. The sine curves, superimposed on the light curves, represent the periodicities found in each observing run.

Fig. 6. Each column from left to right corresponds to the first, second and third subset, respectively. Both periodicities found in each subset are superimposed on the lights curves of Fig. 5. The aliases of both periodicities as well as the harmonics of $\mathrm{P}_{\mathrm{sh}}^{-}$ are evident. As seen in Fig. 6a–6c, the aliases are strong, and they dominate the periodogram in the vicinity of P_{sh}^{-} and bias its estimate. We therefore first fitted the 4-d period, then subtracted it and finally ran periodogram analysis again. Once more the aliases appeared stronger. We also applied the same procedure in the whole of the OHL observing nights (i.e. subset 1 and 2) but again we could not detect f_1 but its $6.17\,\mathrm{cd}^{-1}$ alias. Treating all light curves as a whole, once more reveals the $1.27\,\mathrm{cd}^{-1}$ alias of f_2 and the $6.17\,\mathrm{cd}^{-1}$ alias of P_{sh}^{-} when period analysis is carried out on the residuals. After subtracting all periodic signals the σ of the measurements was found to be 0.048 ± 0.007 mag.

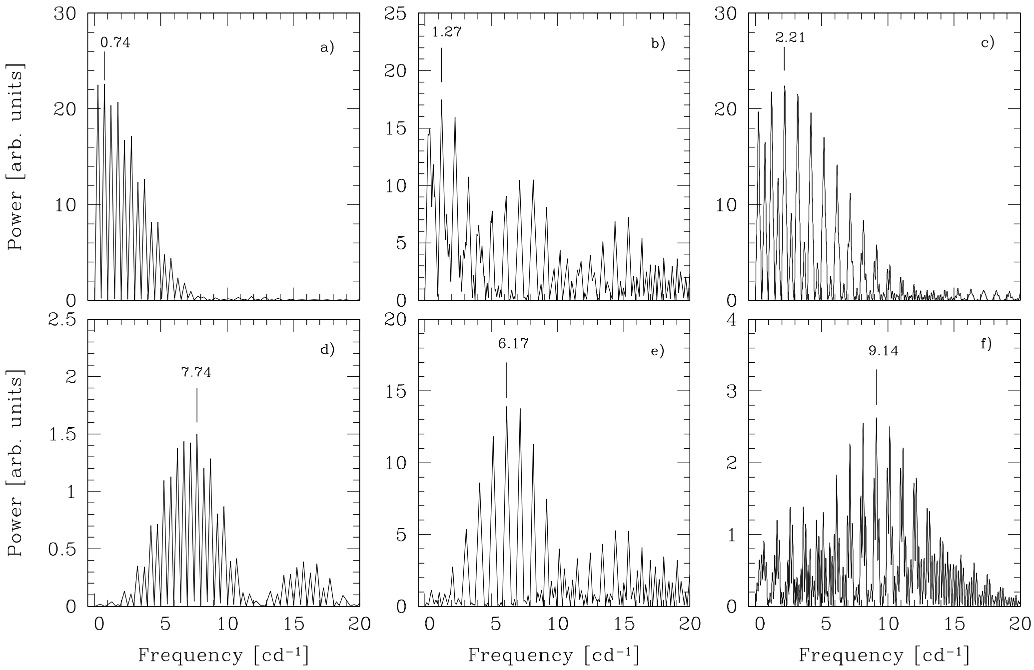

Figure 6: V751 Cyg power spectra with the dominant frequencies indicated. a, b and c correspond to the power spectra of the first, second and third subset, respectively. d, e and f are the power spectra of the residuals of the first, second and third subset, respectively.

The power spectra of CVs show so called "red noise", thought to originate from the flickering through a shot noise-like process. This is demonstrated by the power-law decrease of the power with the frequency which is represented by a line in log-log scale. In this way, the power-law index γ is used for the characterisation of flickering activity. According to theoretical studies, $\gamma = 2$ corresponds to shots of infinite rise-time and exponential decay, shots of totally random duration and shape. Lower values correspond to shots with different duration and distribution, that are neither random nor stable. For more information on "red noise" and γ interpretation, we refer to Papadaki et al. (2006) and references therein. "Red noise" is also present in our case and therefore the linear part, from 100 cd^{-1} on, was fitted by a least squares fit. We found $\gamma = 1.41 \pm 0.03$ for the OHL observing runs, $\gamma = 1.17 \pm 0.03$ for the KR observing run and $\gamma = 1.29 \pm 0.02$ for all runs. However, due to the noisy character of the power spectra, small changes in the fitting interval cause changes in the value of γ up to 0.1, 0.15 and 0.13 for the OHL, KR and all observing runs, respectively. These more realistic γ errors should be adopted instead. It has to be mentioned that when Patterson et al. (2001) applied the same procedure for their power spectra they found $\gamma = 2$. In our case the lower γ suggests a different shot distribution.

7 V516 Cyg

Despite its early discovery as a variable star (Hoffmeister, 1949) V516 Cyg was only noticed to be a DN by Meinunger (1966). It was decades later, that the first optical spectrum was obtained and V516 Cyg was confirmed to be a DN (Bruch & Schimpke, 1992). The spectrum showed a strong blue continuum with Balmer and He I lines in emission. The Balmer emission lines were superimposed on absorption troughs, characteristic of DN declining from (or rising to) an outburst. The first $BVRI$ photometric study during the decline from outburst was conducted by Spogli et al. (1998), who favoured an outside-in outburst. Spogli et al. (2000) covered a complete outburst cycle. The long-term light curves can be found in the two aforementioned studies. The light curve of V516 Cyg during the whole outburst cycle pointed to the SS Cyg subclass of CVs.

V516 Cyg was observed at UC during 5 nights. No filter was used and the exposure time varied between 30 and 60 sec. The light curves are shown in Fig. 7. During the first observing run the system was at the peak of an outburst, confirmed by AAVSO long-term light curves. During the second observing run the system was returning to quiescence, having reached it the last night. The magnitude difference between the two states was ≈2.5 mag.

Frequency analysis was applied to the whole dataset, as well as to the two observing runs independently, but no dominant periodicity was revealed. The system's decrease in brightness was followed by an increase in σ, found to be 0.0129±0.0004 mag in outburst. Although still greater, the σ of the measurements during quiescence, in reality, is not much different than that of outburst since the errors on a single measurement have increased almost proportionally to σ. This implies that there is probably no change in the level of flickering.

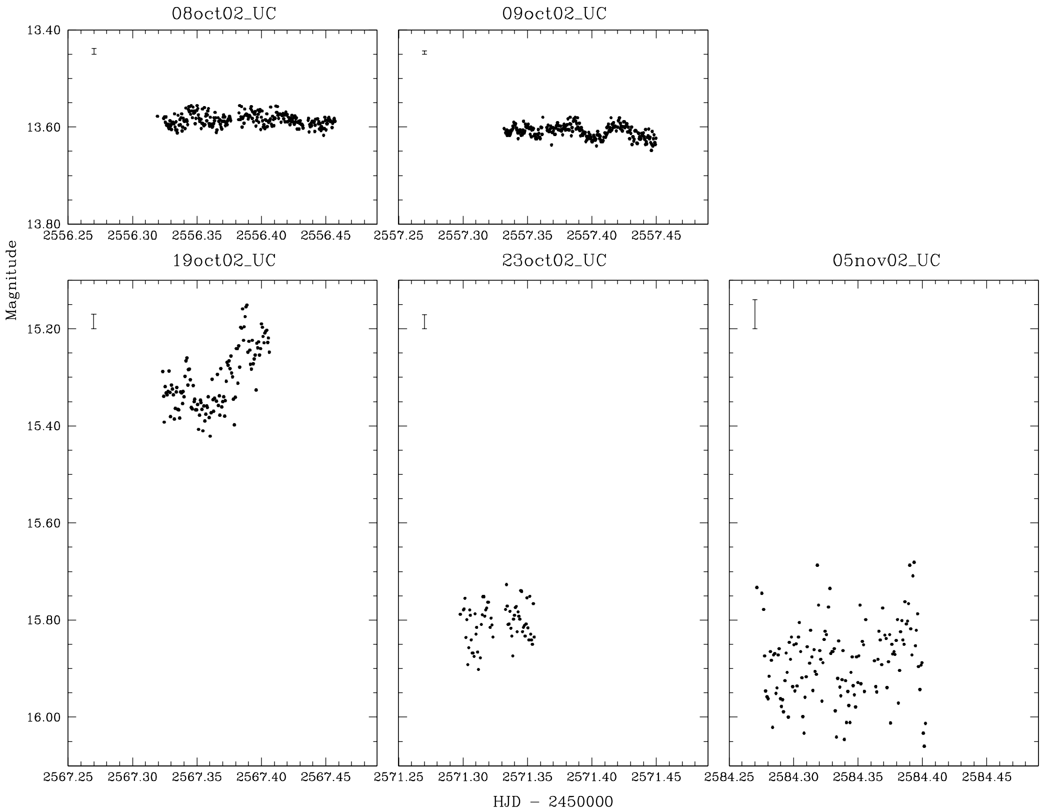

Figure 7: V516 Cyg light curves. In the upper left corner of each light curve the error on a single measurement is shown.

8 GZ Cnc

GZ Cnc (Tmz V034, RX J0915.8+0900) was discovered by Takamizawa (1998) and identified as a ROSAT source by Bade et al. (1998). Jiang et al. (2000) obtained the first optical spectrum which confirmed it as a CV. Some noticeable brightenings (Kato et al., 2001) stimulated interest in monitoring it, and the detection of several outbursts confirmed it as a DN (Kato et al., 2001, 2002). Photometry during the decline from outburst (Kato et al., 2001) suggested that GZ Cnc should be a long-period DN, probably of the SS Cyg subtype. This was based on the facts that GZ Cnc showed no superhumps, had a low outburst amplitude and a slow rising at a rate similar to CVs of the SS Cyg subtype. Their dataset consists of 3 nights, the longest one spanning ≈3.3 h. The long-term light curve of GZ Cnc was studied by Kato et al. (2002): GZ Cnc showed anomalous clusterings of outbursts in 2002 – in contrast to earlier years – and these authors associated this with the behaviour seen in some intermediate polars (IPs). This would result in a period greater than 3 h. However, radial velocities of the Hα emission line revealed the system's $P_{\rm orb}$ of 2.118±0.007 h (Tappert & Bianchini, 2003). The same study also favoured the

IP model due to the strength of the HeII line and the appearance of an absorption component during the rise to outburst. They summed up that even though there were strong indications that GZ Cnc could be an IP, these indications could by no means be conclusive. Both high-speed photometry and time-resolved spectroscopy could clarify its classification.

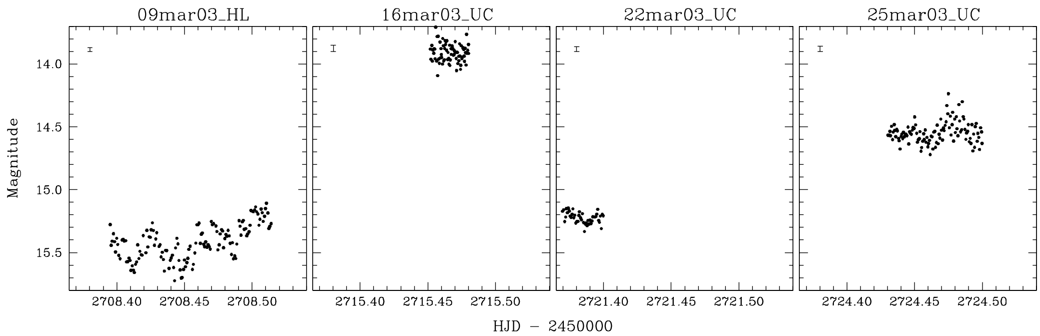

Figure 8: GZ Cnc light curves. In the upper left corner of each light curve the error on a single measurement is indicated.

This dataset consists of 1 night of observing at OHL and 3 nights at UC, no filter was used and the exposure time varied between 50 and 60 sec. Since no well defined magnitudes exist, the ones from the USNO-A2 catalogue were used for computing the system's magnitude. Fig. 8 shows the light curves.

The system is caught during one of its frequent outbursts but unfortunately our coverage is not complete enough to reveal any periodicities. After excluding the two shortest nights, there is a weak signal at frequency 6.5 cd^{-1} (3.7 h). However, the folding of the light curves on this frequency and our maximum coverage per night which does not exceed 2.8 h make us quite unsure of its reality. The σ of the measurements is 0.084±0.041 mag.

9 TY Psc

The outbursting character of the SU UMa system TY Psc was first studied from AAVSO light curves (Szkody & Mattei, 1984). General and mean outburst characteristics can be found in Table 1 and Table 2 of the same study. A 1.7-h photometric modulation was reported by Robinson (1983). UV and optical spectra revealed that TY Psc is a weak source in both cases (Szkody, 1985). The optical spectra of the same study showed broad absorption dips around the emission lines in the blue region of the spectrum, thus indicating a substantial contribution of the WD. Infrared light curves (Szkody & Feinswog, 1988) showed a variation at 46 min, which they identified as the ellipsoidal variation caused by the secondary star, a conclusion they supported with the fact that the system showed superhumps with a period of 101 min. This would mean that P_{orb} would be shorter and 92 min which is the double of the ellipsoidal variation would be a good fit. Also their $J-H$ values supported a large contribution of the secondary star. The same authors gave a rough estimate of the inclination at 55°. Spectrophotometry by Thorstensen et al. (1996) confirmed the strong WD contribution as noted before by Szkody (1985), as well as a $P_{\rm orb}$ of 98.4 min, from both radial velocities and photometry. Both the orbital modulation and double-peaked emission lines pointed to a rather high inclination, while the hot spot was also identified in the light curve. Ciardi et al. (1998) performed time-resolved near-infrared broadband photometry and concluded that the secondary star contributed less than 20% of the infrared flux, therefore opposing the idea of the ellipsoidal variation (Szkody & Feinswog, 1988). Their light curve was quite similar to the optical one (Thorstensen et al., 1996). This resemblance was interpreted as a result of the hot spot in the accretion disc dominating the emission and not as the secondary star contribution, which they found insufficient. Last, the superhump period of 101.9 min was confirmed through observations during the 2000 superoutburst (Kunjaya et al., 2001).

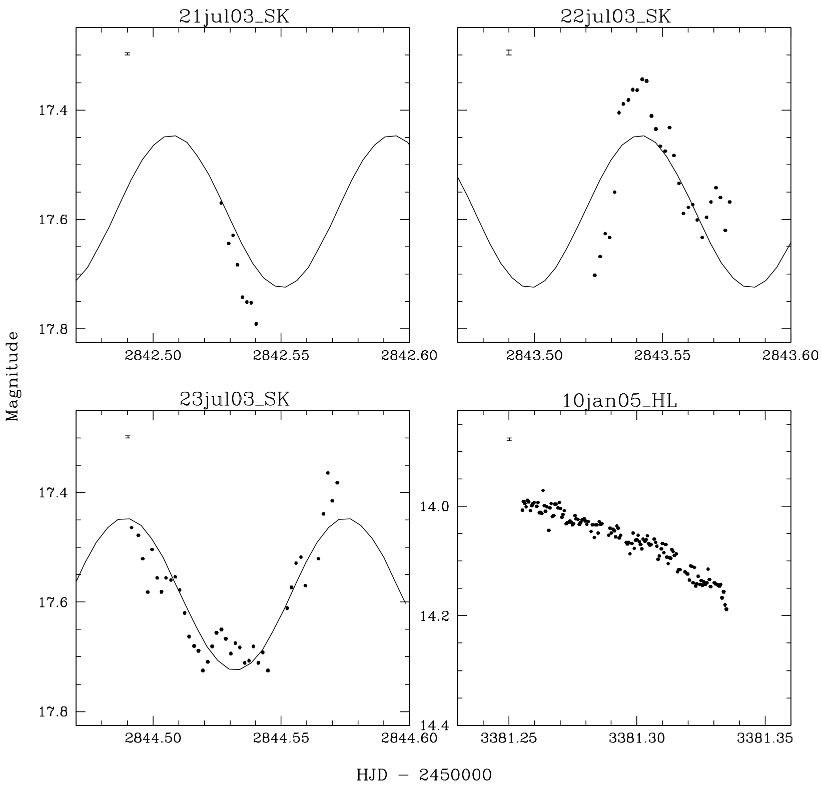

Figure 9: TY Psc light curves. In the upper left corner of each light curve the error on a single measurement is indicated. The light curves on top and bottom left correspond to quiescence, while the light curve on bottom right to outburst.

TY Psc was observed at both SK and OHL for 3 and 1 nights, respectively. The exposure time was 40–120 sec and no filters were used. Fig. 9 shows the light curve during the SK observing run with TY Psc in quiescence (top row and bottom row on the left), and during the OHL observing run with TY Psc in outburst (bottom row on the right).

Frequency analysis was performed during quiescence (SK light curves) and a frequency of 11.60±0.02 cd^{-1} with a semi-amplitude of 0.14±0.01 mag was found. This frequency corresponds to 14.63 cd^{-1}, an alias of the orbital frequency, and the power spectrum reveals the large number of aliases around this frequency, including the orbital one. Our periodicity of 2.01 h is overplotted on the light curves of Fig. 9. For a check we also tried to fold the light curves on $P_{\rm orb}$, something that gave subtle differences. Concerning the single night in outburst, we did not use it in the analysis. The corresponding light curve in Fig. 9 also indicates that $P_{\rm orb}$ would not fit. The system, as confirmed by AAVSO light curves, had just started its decline from the outburst peak. Such a fast decline (≈3 d for this system) seems to temporarily alter the morphology of the light curve.

After removing the periodicity from the SK light curves and the trend from the OHL one, we obtained $\sigma = 0.042 \pm 0.003$ mag and 0.012± 0.004 mag for the quiescence and outburst, respectively. This implies a decrease in the level of flickering since the errors of the measurements have not changed significantly.

10 ASAS J002511+1217.2

ASAS J002511+1217.2 (1RXS J002510.8+121725) was discovered by Pojmanski (2002) and the All-Sky Automated Survey (ASAS). It was also detected by ROSAT (Voges et al., 1999). Upon an alert of a dramatic increase in brightness, astronomers started following the object for a 2-month period. The long-term light curve, first presented by Golovin et al. (2005), revealed that ASAS J002511+1217.2 was an excellent WZ Sge candidate. The same light curves, accompanied by spectroscopic observations, were extensively studied by Templeton et al. (2006) who classified it as a new WZ Sge star. WZ Sge stars have infrequent large-amplitude outbursts, orbital periods around 2 h, show superhumps, and a slow decline from maximum light to quiescence during which echo outbursts are occasionally formed. Echo outbursts resemble DN outbursts and appear directly after the main outburst. They are of about similar amplitude and recurrence time while after their complete cessation the system slowly returns to quiescence (Patterson et al., 2002). ASAS J002511+1217.2 does not lack any of these characteristics and the results of Templeton et al. (2006) will now be briefly presented.

The system's light curve spans three months (mid-September 2004 – mid-December 2004) and during that period the system declined by ≈7 mag. The early abrupt decline was followed by one echo outburst and the decay time to quiescence lasted ≈90 days. Time-series CCD photometry during the early outburst showed clear superhumps at 81.9 min shifting around this value as the system faded. During the quiescent state, just prior to the echo outburst, variations at 81.6 min were detected. During the echo outburst there appeared to be weak variations of the same period as the original superhumps. A few nights of photometry during the late outburst (after the echo outburst) showed signals at periods nearly the same as the superhumps, however, it was not as easy to distinguish due to the increased photometric noise. Time-series spectroscopic observations, well into the object's decline, yielded a $P_{\rm orb}$ of 82±5 min, albeit not too precise. Narrow and broad components in the emission-line spectra indicated the presence of multiple emission regions.

ASAS J002511+1217.2 was observed during 3 nights at OHL, right after the 2004 echo outburst. The exposure varied between 15 and 60 sec, and the light curves are shown in Fig. 10.

Our observations lying after the end of the echo outburst show similar results with Templeton et al. (2006). We find a frequency of 13.42±0.12 cd^{-1} with a semi-amplitude of 0.08±0.01 mag and an alias of the superhump modulation. However, the folding is not satisfactory. The residual σ of the measurements is 0.070±0.017.

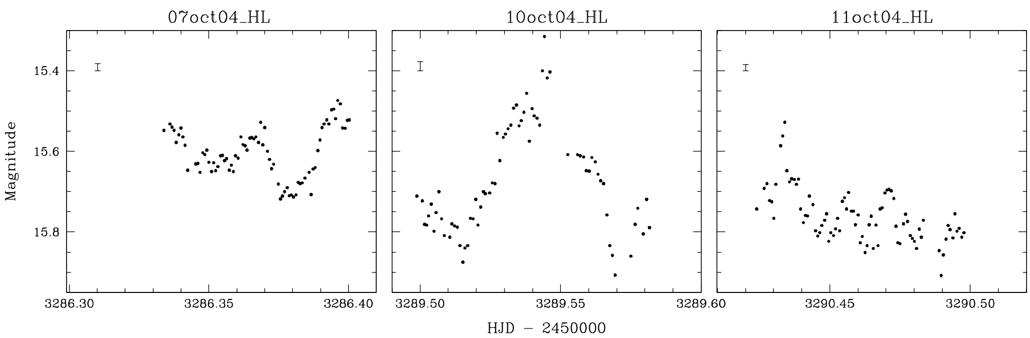

Figure 10: ASAS J002511+1217.2 light curves. In the upper left corner of each light curve the error on a single measurement is indicated.

11 V1315Aql

V1315 Aql (KPD 1911+1212, SVS 8130) was discovered and suspected as a variable star by Metik (1961). Later on, based on a spectrophotometric study, Downes et al. (1986) classified this object as an eclipsing CV, with an eclipse depth up to 1.8 mag in V. $P_{\rm orb}$ was found to be 3.35 h. Apart from Balmer and HeI emission lines the spectra showed strong high-excitation lines. Even though the HeII λ4686 was totally eclipsed, the Balmer lines were not. A prominent absorption component was visible at phase 0.5.

These spectral characteristics, combined with the occurrence of single-peaked emission lines despite the system's high inclination (Szkody & Piche, 1990), uncommon at that time, provided the impetus for the system's follow up and the emergence of a new sub-class of NL CVs, the SW Sex stars. A detailed spectroscopic study by Dhillon et al. (1991) showed that the spectra of V1315 Aql have: (1) narrow single-peaked Balmer and HeI lines exhibiting a double-peaked structure near phase 0.5 and (2) high-excitation lines, remaining single-peaked throughout the orbit and being totally eclipsed in contrast to Balmer and HeI lines. They presented the first Doppler maps which showed a contaminating emission around phase 0.75 and no disc emission. They connected this to the large phase shifts seen in the radial-velocity measurements of all emission lines. Even though the subsequent Doppler maps presented by Kaitchuck et al. (1994) appeared quite similar, there was disagreement concerning the origin of the HeII peak emission. Although Dhillon et al. (1991) did not find it to coincide with the expected location of the WD, Kaitchuck et al. (1994) did. In this way they drew the conclusion that HeII is mostly emitted from a region very close to the WD and is therefore a good indicator of the WD orbital motion.

Further spectroscopy (Friend et al., 1988; Smith et al., 1993) showed a strong absorption feature at the OI triplet $\lambda 7773$. A detailed study by Smith et al. (1993) concluded that this feature must arise from some absorbing material that is distributed in a non-axisymmetric manner. This asymmetry seemed to be confined only to OI. Infrared spectroscopy showed no evidence for the secondary star (Dhillon et al., 2000). For an analytic presentation of a model that could describe the characteristics and peculiarities of V1315 Aql, as well as previous attempts on the same subject, see Hellier (1996) and references therein. In short, the model combines the occurrence of both disc overflow and a strong wind, which might result from high mass-transfer rate.

V1315 Aql was observed at SAAO (4 nights), at SK (3 nights) and at KR (1 night). At SK observing run the Johnson-R filter was used, while the rest of the observing runs were done without filter. The exposure time was 40-60 sec. The light curves are shown in Fig. 11.

V1315 Aql was observed during two periods, August 2003 and August–September 2004. In total, the system was caught during nine eclipses but, only six of them were fully covered and are therefore used for further analysis. The timings of mid-eclipse, determined by fitting a Gaussian to the lower half of the eclipses, are given in Table 4. The same table also includes all previously reported minima and their corresponding cycle number E. The refined ephemeris resulting from all available eclipse timings is:

$$T_{\mathrm{mid-ecl}}[\mathrm{HJD}] = \underset{\pm 0.0001}{2445902.7007} + \underset{\pm 0.000000005}{0^{\mathrm{d}}.139689959}\,E$$

Fig. 12 shows the $O-C$ diagram of all available minima. O represents the observed times of minima and C the calculated ones according to the ephemeris. In agreement to all previous studies, no evidence of any kind of curvature or trend is found in the $O-C$ diagram. This means that in the now even longer baseline of 20 years there is no indication of a change in the system's period.

A look at Fig. 12 shows that there is a large scatter of data points at the first and last block of data. However, concerning the last block belonging to our observations,

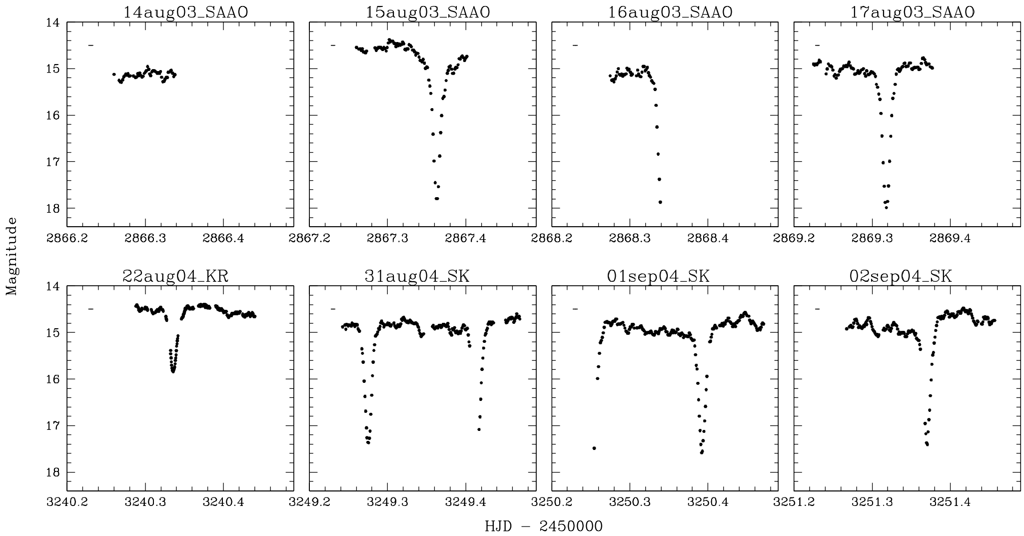

Figure 11: V1315 Aql light curves. In the upper left corner of each light curve the error on a single measurement is indicated.

the variations we are looking at are of the order of 40–50 sec, i.e. of the size of the exposure times and therefore they should not be of any significance. Unfortunately, no errors are given on any of the previous studies and so we can not reach any conclusion about the even larger scatter of the first block.

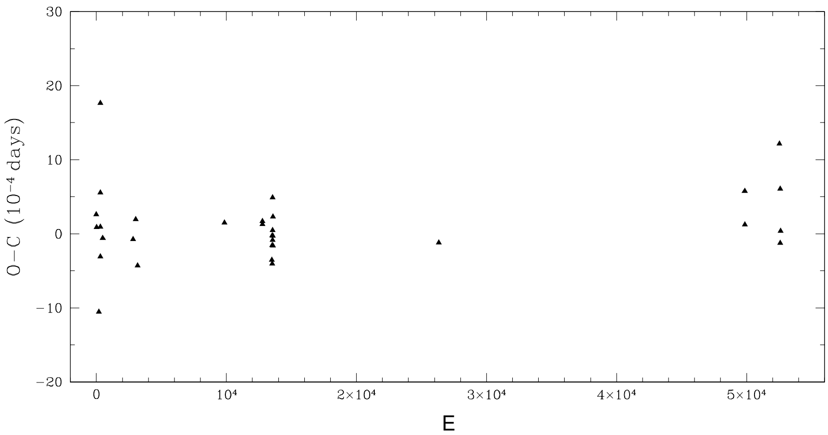

Figure 12: $O-C$ diagram for the timings of mid-eclipse of all available data (see Table 4).

The application of frequency analysis, after removal of the eclipse data, gives a frequency of $5.14627 \pm 3 \cdot 10^{-5}\,\mathrm{cd}^{-1}$ an alias of the orbital frequency. We also searched for long-term periodicities, but none was evident. The σ of the measurements is

Table 4: Eclipse timings of V1315 Aql

$T_{\mathrm{mid-ecl}}$ (HJD-2445000)	E	Source
902.84065	1	Downes et al. (1986)
906.75180	29	Downes et al. (1986)
928.82167	187	Annis (1986)
944.74793	301	Downes et al. (1986)
944.88716	302	Downes et al. (1986)
945.72697	308	Annis (1986)
945.86459	309	Downes et al. (1986)
971.70748	494	Downes et al. (1986)
1295.78815	2814	Annis (1986)
1324.70424	3021	Annis (1986)
1344.67928	3164	Annis (1986)
2279.62471	9857	Dhillon et al. (1991)
2686.54156	12770	Dhillon et al. (1991)
2686.68121	12771	Dhillon et al. (1991)
2788.37501	13499	Dhillon et al. (1991)
2790.47069	13514	Dhillon et al. (1991)
2791.44839	13521	Dhillon et al. (1991)
2793.40380	13535	Dhillon et al. (1991)
2794.52177	13543	Dhillon et al. (1991)
2795.49947	13550	Dhillon et al. (1991)
2796.47787	13557	Dhillon et al. (1991)
2798.43327	13571	Dhillon et al. (1991)
2800.38867	13585	Dhillon et al. (1991)
2801.36637	13592	Dhillon et al. (1991)
4579.6195	26322	Hellier (1996)
7867.36291	49858	This study
7869.31812	49872	This study
8240.33572	52528	This study
8249.27527	52592	This study
8250.39206	52600	This study
8251.37005	52607	This study

0.117 ± 0.034 mag.

As previously mentioned, V1315 Aql undergoes eclipses of around 1.8 mag in V. In our case the eclipse depth is found around 3.2 and 2.6 mag in the 2003 (data obtained without filter) and R-band 2004 observing run, respectively. The only exception is the eclipse depth of the night of 22$^{\mathrm{nd}}$ August 2004 (data obtained without filter), with an eclipse depth that is remarkably smaller at 1.5 mag, half or less than half of the rest of the nights. In Fig. 13 the out-of-eclipse magnitude has been shifted to zero and the variable eclipse depth is readily estimated. Variable

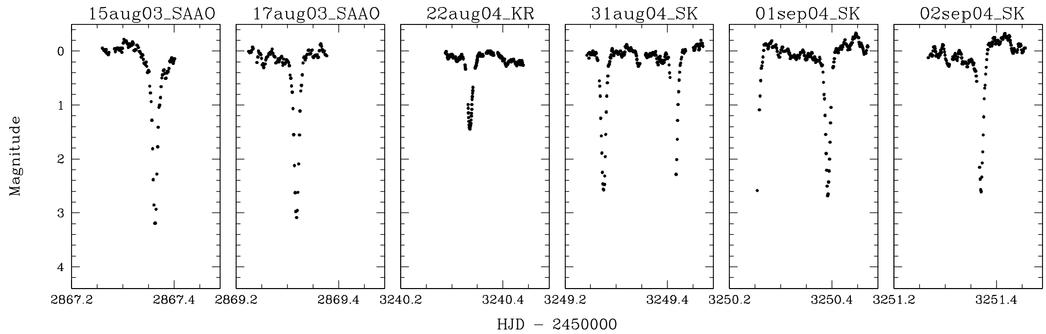

Figure 13: V1315 Aql eclipse light curves with the out-of-eclipse magnitude shifted to zero. The eclipse depth varies between 1.5 and 3.2 in the two extreme nights.

eclipse depth has also been reported for DW UMa (Stanishev et al., 2004) and PX And (Stanishev et al., 2002). In DW UMa it was attributed to the change between high and low state of the accretion disc radius and therefore the surface of the eclipsed accretion disc. However, in our study the unique low-depth eclipse makes it hard to investigate further and to draw firm conclusions. Even if we tried to associate the eclipse depth with the system luminosity we can directly see that between the two extreme nights of 15 August 2003 and 22 August 2004 where the eclipse depth is ≈ 1.5 and 3.2 mag, the out-of-eclipse magnitude is the same (see Fig. 11). In PX And the eclipse-depth was suggested to be modulated with the precession period of the accretion disc. However, in the case of V1315 Aql no longer-term modulation has been suggested so far.

12 LN UMa

LN UMa (UMa7, PG 1000+667) was discovered in the Palomar-Green survey (Green et al., 1986) and, based on its spectral characteristics, was classified as a NL CV (Ringwald, 1993). Ringwald (1993) found a period of 4.06 h. However, the spectrophotometric study of Hillwig et al. (1998) revealed a refined $P_{\rm orb}$ of 3.47 h through Hβ radial velocities. Their multi-year photometry (1400 days covering 1 point every 4.7 days) showed two drops of 3 magnitudes (Hillwig et al., 1998; Honeycutt & Kafka, 2004). Given $P_{\rm orb}$ and the low states, LN UMa was identified as a VY Scl star. Not much later, a spectroscopic search for new SW Sex stars revealed that LN UMa is also part of this interesting subclass of CVs (Rodriguez-Gil et al., 2007).

Our dataset consists of five observing nights, three at SK and two at UC. At SK we observed using the Johnson-R filter while the UC observing run was done without filter. The exposure time varied between 60 and 80 sec. The light curves are shown in Fig. 14.

After checking the long-term light curves of our system from AAVSO it is clear that the UC observing run is placed during the normal high state, but this is not

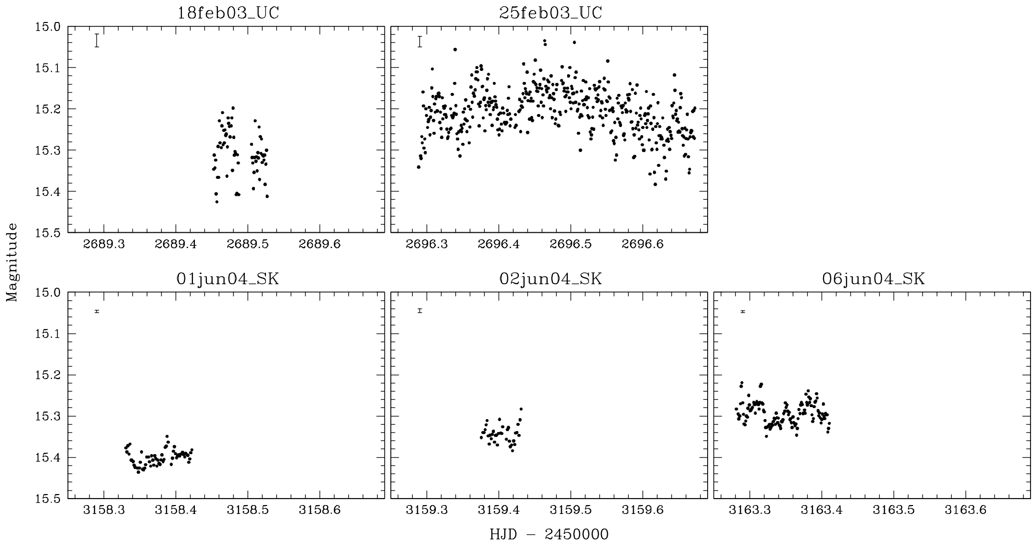

Figure 14: LN UMa light curves. In the upper left corner of each light curve the error on as single measurement is shown.

evident for the SK observing run. However, the trend of the AAVSO light curves points to the normal high state for the SK run as well. As seen in Fig. 14, the atmospheric conditions for the SK observing run are much better than the UC one, with the error being greater in the UC run. The σ of the measurements of LN UMa is found 0.055±0.001 mag for the UC and 0.022± mag for the SK observing run. The last value is the one that should be trusted.

Period analysis of all of our datasets as well as the two individual observing runs did not reveal the spectroscopic $P_{\rm orb}$ or any other modulations. The high amplitude flickering of the longest observing night, covering more than two orbits, could easily mask any underlying periodicity.

13 Summary

The results of this study can be summarised as follows:

EI UMa For the first time we confirm through photometry the spectroscopic $P_{\rm orb}$ of 6.4 h. Its rather low semi-amplitude of 0.0212 mag made its direct detection in 2002 more difficult and was probably the reason for its non-detection so far. Moreover, in 2002 the system exhibits a gradual increase in brightness reaching a maximum of 0.6 mag and a high amplitude unstable modulation. The increase in brightness is followed by a decrease in the standard deviation σ of the measurements, and probably of the level of flickering.

V844 Her The spectroscopically defined $P_{\rm orb}$ could not be detected. The same applies for $P_{\rm sh}^{+}$ but this was expected since the system was in quiescence. AAVSO long-term light curves confirm that our second observing run lies just before the onset of an outburst and our third one lies just after the end of the same superoutburst.

V751 Cyg We have detected the two previously reported photometric signals P_{sh}^{-} and P_{wob}, albeit only their aliases and harmonics in some cases. In contrast to Patterson et al. (2001) who found $\gamma = 2$, we obtained 1.29 which implies that the flickering activity has changed and in our case the shot-noise follows a different distribution.

V516 Cyg The system was observed at the peak of an outburst and during its decline, until it reached its quiescent state. Between the two extreme states a magnitude difference of 2.5 mag was observed. No dominant periodicity could be detected. The decrease in brightness was followed by an increase in flickering activity, expected since the accretion disc returns to its normal smaller size and the relative contribution of the BS, major cause of the flickering activity, increases.

GZ Cnc No periodicity could be detected during one of the system's frequent outbursts.

TY Psc This system was observed during quiescence and during the initiation of decline from the peak of an outburst. We detected P_{orb} during quiescence but not in outburst. The amount of flickering decreased with increasing brightness.

ASAS J002511+1217.2 Our results resemble those of Templeton et al. (2006) which were also obtained after the echo outburst. The light curves exhibit high amplitude flickering and show two possible signals: at 13.42 cd^{-1} and at an alias of the superhump modulation.

V1315 Aql Our observations covered nine more eclipses which combined with the previously reported mid-eclipse timings, provide a refined orbital ephemeris. The $O-C$ shows that during the 20-year baseline there is no trend or curvature and therefore no change in the system's period. The eclipse depth varies between 2.6 and 3.2 mag with the exception of one night where it has a remarkably smaller value of 1.5 mag. For the moment no association between the brightness level and the eclipse depth can be made because the two nights with the extreme values of the eclipse depth (1.5 and 3.2 mag) share the same out-of-eclipse magnitude.

LN UMa Our observing set is probably placed during the system's normal high state and does not reveal the spectroscopic P_{orb} or any other modulation.

14 The data

14.1 Tables

The files `table1.dat`–`table4.dat` are ASCII files of the same tables as presented in this manuscript.

14.2 Light curve data

The files `fig2.dat`–`fig14.dat` (the same numbering as in the manuscript is followed) are ASCII files with the light curves of EI UMa, V844 Her, V751 Cyg, V516 Cyg, GZ Cnc, TY Psc, ASAS J002511+1217.2, V1315 Aql and LN UMa, respectively. They give the HJD and differential magnitude of each CV.

Moreover, the instrumental magnitudes (i.e. those before the application of differential photometry) of each CV and its comparison stars are given in ASCII files with HJD, magnitude and magnitude error. Those files are `table5.dat`–`table13.dat` for EI UMa, V844 Her, V751 Cyg, V516 Cyg, GZ Cnc, TY Psc, ASAS J002511+1217.2, V1315 Aql and LN UMa, respectively. The first column gives the HJD, the second and third give the instrumental magnitude and corresponding error of the CV, the fourth and fifth give the instrumental magnitude and corresponding error of the first comparison star, the sixth and seventh give the instrumental magnitude and corresponding error of the second comparison star and so on.

14.3 Calibrated frames

The directories `EIUMa_frames, V844Her_frames, GZCnc_frames, V1315Aql_frames, V516 Cyg_frames, LNUMa_frames, V751Cyg_frames, TYPsc_frames` and `ASAS_frames` contain the calibrated frames of each target as compressed FITS files. The naming convention in each CV directory is {UTdate}_{sequence number}.fits.bz2 . UT date represents the beginning of each observing night.

Acknowledgments

The first author carried out the bulk of the observations.

We are grateful to the following persons for the generous allocations of time: Prof. Klaus Reif and Prof. Wilhelm Seggewiss at the Observatorium Hoher List, Dr. Iosif Papadakis, and Dr. Pablo Reig at Skinakas Observatory.

Skinakas Observatory is a collaborative project of the University of Crete, the Foundation for Research and Technology-Hellas, and the Max–Planck–Institut für extraterrestrische Physik. This paper uses observations made at the South African Astronomical Observatory (SAAO).

We wish to thank Dr. H.W. Duerbeck for comments that greatly improved the quality of the manuscript.

This work has been partly supported by grant FWO-G.0332.06 of the Belgian Fund for Scientific Research. C.P. gratefully acknowledges a doctoral research grant by the Belgian Federal Science Policy Office (Belspo).

References

Annis, J. T. 1986, IBVS, 2858, 1

Antipin, S. V. 1996, IBVS, 4360, 1

Bade, N., Engels, D., Voges, W., et al. 1998, A&AS, 127, 145

Bruch, A. & Schimpke, T. 1992, A&AS, 93, 419

Ciardi, D. R., Howell, S. B., Hauschildt, P. H., & Allard, F. 1998, ApJ, 504, 450

Cook, M. C. 1985, MNRAS, 215, 81P

Dhillon, V. S., Littlefair, S. P., Howell, S. B., et al. 2000, MNRAS, 314, 826

Dhillon, V. S., Marsh, T. R., & Jones, D. H. P. 1991, MNRAS, 252, 342

Downes, R., Hoard, D. W., Szkody, P., & Wachter, S. 1995, AJ, 110, 1824

Downes, R. A., Mateo, M., Szkody, P., Jenner, D. C., & Margon, B. 1986, ApJ, 301, 240

Friend, M. T., Smith, R. C., Martin, J. S., & Jones, D. H. P. 1988, MNRAS, 233, 451

Golovin, A., Price, A., Templeton, M., et al. 2005, IBVS, 5611, 1

Green, R. F., Ferguson, D. H., Liebert, J., & Schmidt, M. 1982, PASP, 94, 560

Green, R. F., Schmidt, M., & Liebert, J. 1986, ApJS, 61, 305

Greiner, J., Tovmassian, G. H., Di Stefano, R., et al. 1999, A&A, 343, 183

Hellier, C. 1996, ApJ, 471, 949

Henden, A. A. & Honeycutt, R. K. 1995, PASP, 107, 324

Herbig, G. H. 1958, ApJ, 128, 259

Herbig, G. H. & Kameswara Rao, N. 1972, ApJ, 174, 401

Hillwig, T. C., Robertson, J. W., & Honeycutt, R. K. 1998, AJ, 115, 2044

Hoffmeister, C. 1949, Astron. Nachr. Erg., 12, 1

Honeycutt, R. K. & Kafka, S. 2004, AJ, 128, 1279

Jiang, X. J., Engels, D., Wei, J. Y., Tesch, F., & Hu, J. Y. 2000, A&A, 362, 263

Kaitchuck, R. H., Schlegel, E. M., Honeycutt, R. K., et al. 1994, ApJS, 93, 519

Kato, T., Dubovsky, P. A., Stubbings, R., et al. 2002, A&A, 396, 929

Kato, T. & Uemura, M. 2000, IBVS, 4902, 1

Kato, T., Uemura, M., Buczynski, D., & Schmeer, P. 2001, IBVS, 5123, 1

Kunjaya, C., Kinugasa, K., Ishioka, R., et al. 2001, IBVS, 5128, 1

Lenz, P. & Breger, M. 2005, Communications in Asteroseismology, 146, 53

Martynov, D. 1958, Perem. Zvezdy, 11, 170

Meinunger, L. 1966, Mitt. Veranderl. Sterne, 3, 137

Metik, L. P. 1961, Peremennye Zvezdy, 13, 364

Munari, U., Zwitter, T., & Bragaglia, A. 1997, A&AS, 122, 495

Papadaki, C. 2008, PhD thesis, Vrije Universiteit Brussel, Brussels, Belgium.

Papadaki, C., Boffin, H. M. J., Sterken, C., et al. 2006, A&A, 456, 599

Patterson, J., Masi, G., Richmond, M. W., et al. 2002, PASP, 114, 721

Patterson, J., Thorstensen, J. R., Fried, R., et al. 2001, PASP, 113, 72

Pojmanski, G. 2002, Acta Astronomica, 52, 397

Ringwald, F. A. 1993, PhD thesis, AA(Dartmouth Coll., Hanover, NH.)

Robinson, E. L. 1983, in Astrophysics and Space Science Library, Vol. 101, IAU Colloq. 72: Cataclysmic Variables and Related Objects, ed. M. Livio & G. Shaviv, 1–14

Robinson, E. L., Nather, R. E., & Kiplinger, A. 1974, PASP, 86, 401

Rodriguez-Gil, P., Schmidtobreick, L., & Gansicke, B. T. 2007, MNRAS, 374, 1359

Scovil, C. 1996, vsnet-obs circulation, No. 4061

Smith, R. C., Fiddik, R. J., Hawkins, N. A., & Catalan, M. S. 1993, MNRAS, 264, 619

Spogli, C., Fiorucci, M., & Raimondo, G. 2000, IBVS, 4977, 1

Spogli, C., Fiorucci, M., & Tosti, G. 1998, A&AS, 130, 485

Stanishev, V., Kraicheva, Z., Boffin, H. M. J., & Genkov, V. 2002, A&A, 394, 625

Stanishev, V., Kraicheva, Z., Boffin, H. M. J., et al. 2004, A&A, 416, 1057

Szkody, P. 1985, AJ, 90, 1837

Szkody, P. & Feinswog, L. 1988, ApJ, 334, 422

Szkody, P. & Mattei, J. A. 1984, PASP, 96, 988

Szkody, P. & Piche, F. 1990, ApJ, 361, 235

Takamizawa, K. 1998, vsnet-obs circulation, No. 10504

Tappert, C. & Bianchini, A. 2003, A&A, 401, 1101

Templeton, M. R., Leaman, R., Szkody, P., et al. 2006, PASP, 118, 236

Thorstensen, J. R. 1986, AJ, 91, 940

Thorstensen, J. R., Patterson, J., Kemp, J., & Vennes, S. 2002, PASP, 114, 1108

Thorstensen, J. R., Patterson, J. O., Shambrook, A., & Thomas, G. 1996, PASP, 108, 73

Vanmunster, T. 1996, vsnet-obs circulation, No. 4075

Voges, W., Aschenbach, B., Boller, T., et al. 1999, A&A, 349, 389

Wilson, J. W., Miller, H. R., Africano, J. L., et al. 1986, A&AS, 66, 323